We are IntechOpen, the world's leading publisher of Open Access books Built by scientists, for scientists

6,900
Open access books available

186,000
International authors and editors

200M
Downloads

Our authors are among the

154
Countries delivered to

TOP 1%
most cited scientists

12.2%
Contributors from top 500 universities

CLARIVATE ANALYTICS
BOOK CITATION INDEX
INDEXED

WEB OF SCIENCE™

Selection of our books indexed in the Book Citation Index
in Web of Science™ Core Collection (BKCI)

Interested in publishing with us?
Contact book.department@intechopen.com

Numbers displayed above are based on latest data collected.
For more information visit www.intechopen.com

Wearable Sensor System for Human Dynamics Analysis

Tao Liu, Yoshio Inoue, Kyoko Shibata and Rencheng Zheng
Kochi University of Technology
Japan

1. Introduction

In clinical applications the quantitative characterization of human kinematics and kinetics can be helpful for clinical doctors in monitoring patients' recovery status; additionally, the quantitative results may help to strengthen confidence during their rehabilitation. The combination of 3D motion data obtained using an optical motion analysis system and ground reaction forces measured using a force plate has been successfully applied to perform human dynamics analysis (Stacoff et al., 2007; Yavuzer et al., 2008). However, the optical motion analysis method needs considerable workspace and high-speed graphic signal processing devices. Moreover, and if we use this analysis method in human kinetics analysis, the devices are expensive, while pre-calibration experiments and offline analysis of recorded pictures are especially complex and time-consuming. Therefore, these devices is limited to the laboratory research, and difficult to be used in daily life applications. Moreover, long-term, multi-step, and less restricted measurements in the study of gait evaluation are almost impossible when using the traditional methods, because a force plate can measure ground reaction force (GRF) during no more than a single stride, and the use of optical motion analysis is limited due to factors such as the limited mobility and line-of-sight of optical tracking equipment. Recently, many lower-cost and wearable sensor systems based to multi-sensor combinations including force sensitive resistors, inclinometers, goniometers, gyroscopes, and accelerometers have been proposed for triaxial joint angle measurement, joint moment and reaction force estimation, and muscle tension force calculation.

As for researches of wearable GRF sensors, pressure sensors have been widely used to measure the distributed vertical component of GRF and analyze the loading pattern on soft tissue under the foot during gait (Faivre et al., 2004; Zhang et al., 2005), but in these systems the transverse component of GRF (friction forces) which is one of the main factors leading to fall were neglected. Some flexible force sensors designed using new materials such as silicon or polyimide and polydimethyl-siloxane have been proposed to measure the normal and transverse forces (Valdastri et al., 2005; Hwang et al., 2008), but force levels of these sensors using these expensive materials were limited to the measurements of small forces (about 50N). By mounting two common 6-axial force sensors beneath the front and rear boards of a special shoe, researchers have developed a instrumented shoe for ambulatory

measurements of CoP and triaxial GRF in successive walking trials (Veltink et al., 2005; Liedtke et al., 2007), and an application of the instrumented shoe to estimate moments and powers of the ankle was introduced by Schepers et al. (2007).

About researches on body-mounted motion sensors, there are two major directions: one is about state recognition on daily physical activities including walking feature assessment (Sabatini et al., 2005; Aminian et al., 2002), walking condition classification (Coley et al., 2005; Najafi et al., 2002) and gait phase detection (Lau et al., 2008; Jasiewicz et al., 2006), in which the kinematic data obtained from inertial sensors (accelerometer or gyroscope) were directly used as inputs of the inference techniques; and another direction is for accurate measurement of human motion such as joint angles, body segment's 3-D position and orientation, in which re-calibration and data processing by fusing different inertial sensors are important to decrease errors of the quantitative human motion analysis. In our research, a wearable sensor system which can measure human motion and ground reaction force will be developed and applied to estimate joint moment and muscle tension force, so we are focusing on the second direction for quantitative human motion analysis. There are growing interests in adopting commercial products of 3D motion sensor system, for example a smart sensor module MTx (Xsens, Netherlands) composed of a triaxial angular rate sensor, a triaxial accelerometer and a triaxial magnetic sensor, which can reconstruct triaxial angular displacements by means of a dedicated algorithm. However, it is sensitive to the effect of magnetic filed environment, and the dynamic accuracy of this sensor is about two degrees, which depends on type of experimental environments.

In this chapter, a developed wearable sensor system including body-mounted motion sensors and a wearable force sensor is introduced for measuring lower limb orientations, 3D ground reaction forces, and estimating joint moments in human dynamics analysis. Moreover, a corresponding method of joint moment estimation using the wearable sensor system is proposed. This system will provide a lower-cost, more maneuverable, and more flexible sensing modality than those currently in use.

2. Wearable GRF Sensor

2.1 Mechanical Design and Dimension Optimization

We developed a wearable multi-axial force sensor with a parallel mechanism to measure the ground reaction forces and moments in human dynamics analysis. First, the parallel mechanism for sensing triaxial forces and moments was introduced. As shown in Fig.1, the sensor is composed of a bottom plane, x-, y- and z-axial load cells, and four balls. When forces and moments are imposed to the bottom plane, they are transferred onto the four support balls. The support balls are connected with three load cells by point contacts. Therefore, only translational forces can be transferred to the corresponding load cells and measured using the strain gauges attached on the load cells. The x-axial load cell can measure F_{X1} and F_{X2}. Similarly, the y-axial load cell measures F_{Y1} and F_{Y2}, while the z-axial load cell measures F_{Z1}, F_{Z2}, F_{Z3} and F_{Z4}. Based on these measured values, the three-axis forces and moments can be calculated by the use of the following equations:

$$F_x = F_{x1} + F_{x2} \tag{1}$$

$$F_y = F_{y1} + F_{y2} \tag{2}$$

$$F_z = F_{z1} + F_{z4} + F_{z2} + F_{z3} \tag{3}$$

$$M_x = (F_{z2} + F_{z3} - F_{z1} - F_{z4})L/2 \tag{4}$$

$$M_y = (F_{z3} + F_{z4} - F_{z1} - F_{z2})L/2 \tag{5}$$

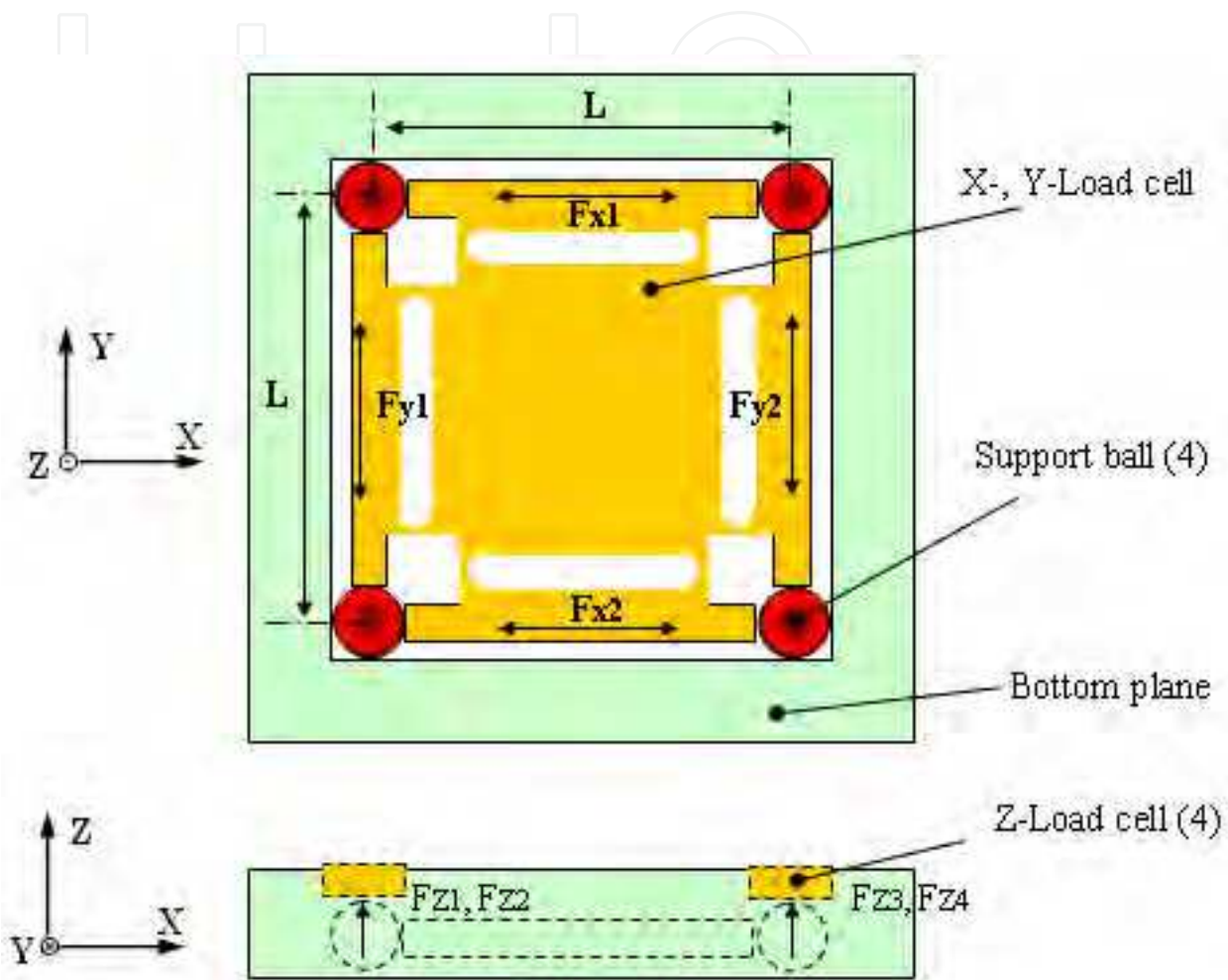$$M_z = (F_{x2} + F_{y2} - F_{x1} - F_{y1})L/2 \tag{6}$$

Fig. 1. Schematic picture for the new Sensor with a parallel Support mechanism. The transverse load cells are composed of two x-axial load cells for measuring F_{x1} and F_{x2} and two y-axial load cells for measuring F_{y1} and F_{y2} respectively. The z-load cells under the four support ball at the four corners (L=100mm) can measure four z-directional forces including F_{z1}, F_{z2}, F_{z3} and F_{z4}.

Figure 2 shows the detail of the load cells. Two strain gauges are attached on the load cell to sense a uniaxial translational force. In order to obtain a high sensitivity, the strain gauges should be distributed on the points where the maximum strains occur. ANSYS, FEA software, was used to perform the static analysis of the load cell. Based on the sensitivity limitation of the strain gauge, the optimal dimensions of the load cell were determined by ANSYS simulations. Figure 3 shows representative results of the static analysis for the load cell.
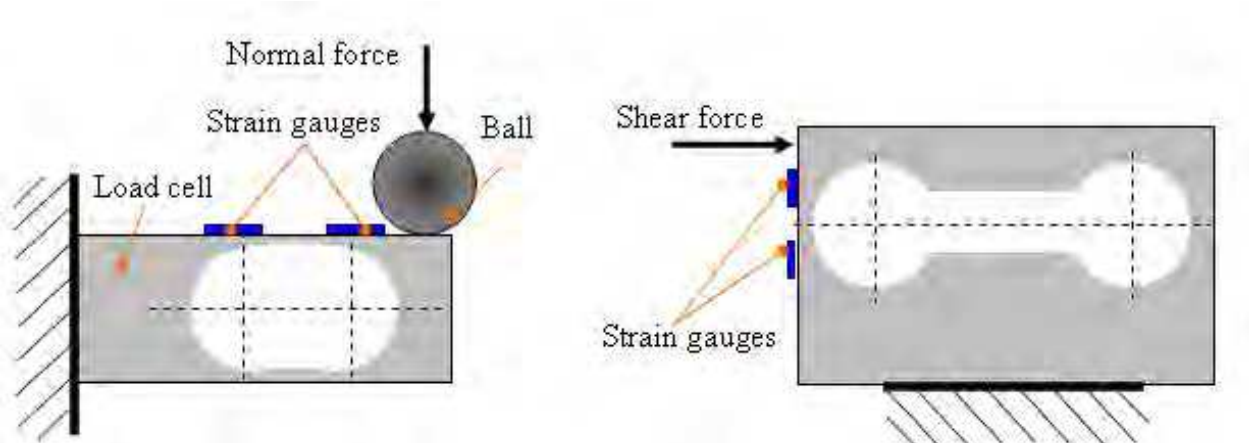
Fig. 2. Schematic of the design of load cell. We put two strain gauges on each load cell's flexible mechanical-body, and a set of two strain gauges is only sensitive to single directional translational force.
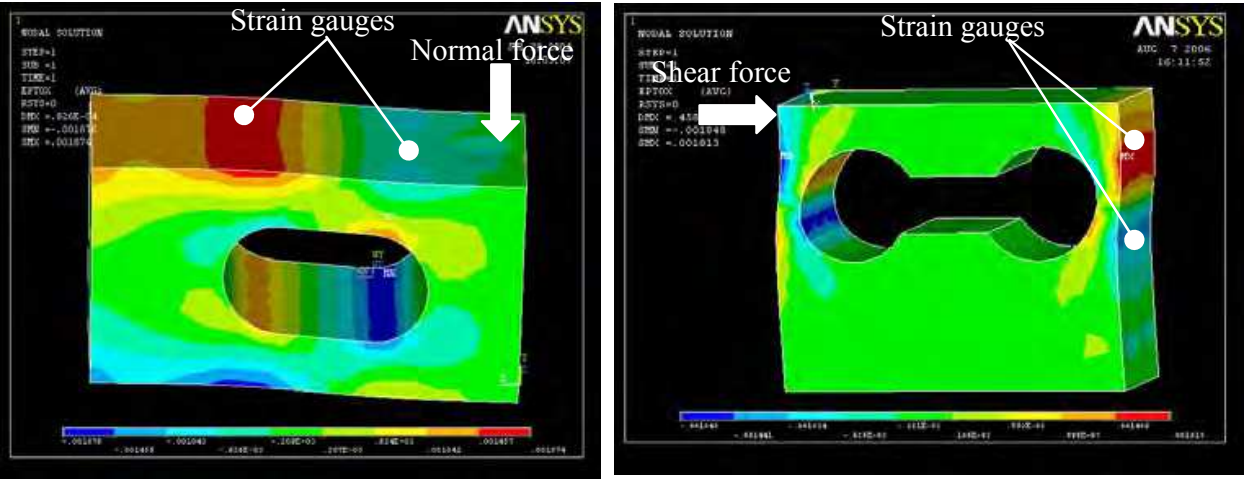

Fig. 3. Result graph of FEA. Finite element method was adopted to optimize the mechanism dimension of the load cells' flexible mechanical-body, and to improve the sensitivity of the force sensor.

As shown in Fig. 4, based on the single load cell obtained by the optimal design, we designed a prototype of the sensor, and the 3D model was constructed using an engineering modeling software of Pro/E. Figure 5 shows the prototype of the load cells in the wearable force sensor, and the flexible beams were made of ultra hard duralumin. Four groups of the strain gauges were used to construct the x- and y-axial load cells, and another four groups were used to make the z-axial load cell. In order to implement a more compact structure, hybrid measurement load cells were adopted for x- and y-directional translational force measurements. This new design can decrease the number of strain gauges and simplify amplifier modules.
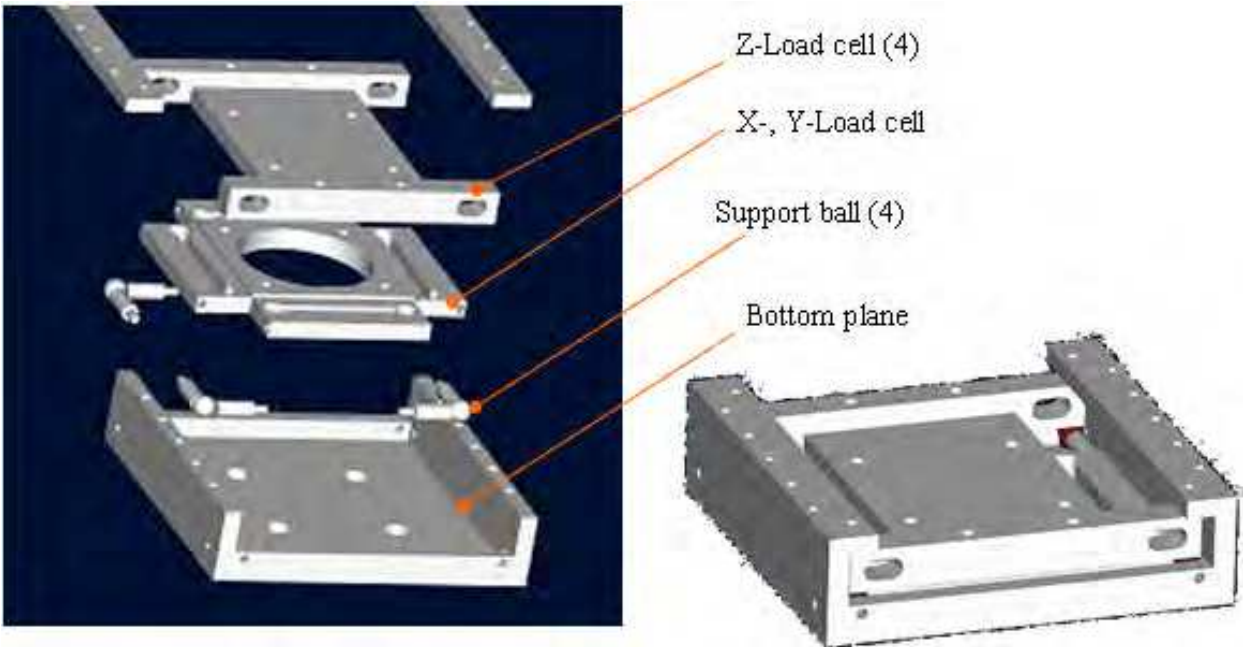
Fig. 4. 3D model of the force sensor using the stimulation model of the force sensor. According to the 3D model, we designed the mechanical structure of the parts in the sensor.

<div align="center">(a)   (b)</div>
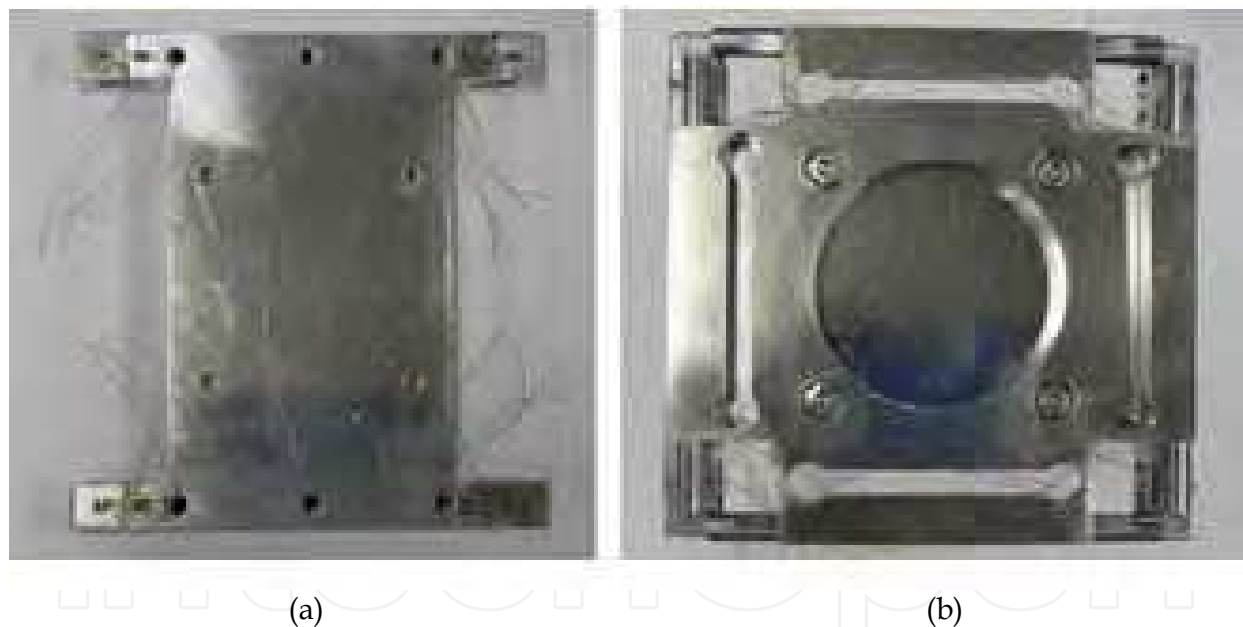
Fig. 5. Mechanical structure of the load cells. (a) The mechanical structure of z-load cell with four sub-load cells which can measure z-direction vertical forces at the four support points. (b) The picture of the x-, y-load cell for the measurements of the horizontal forces.

2.2 Electrical System Design and Integrated Sensor System

As shown in Fig. 6, an integrated electrical system was developed and incorporated into the force sensor. The strains due to forces applied on the flexible body are converted to the resistance changes. Then the resistance changes are converted to the voltage signals by the conditioning modules, and are amplified by the amplifier modules. The amplified voltage

signals X_i (i=1, 2, 3…8) are input into a personal computer through serial port (RS232) after A/D conversion using a micro-computer system. Since eight channels of the strain gauges were used (four groups for x- and y-directional forces and another four groups z-directional forces), there are eight channels of the voltage signals. A program specially developed in MATLAB was used to sample the eight channels of the voltage signals and calculate the forces and the moments.
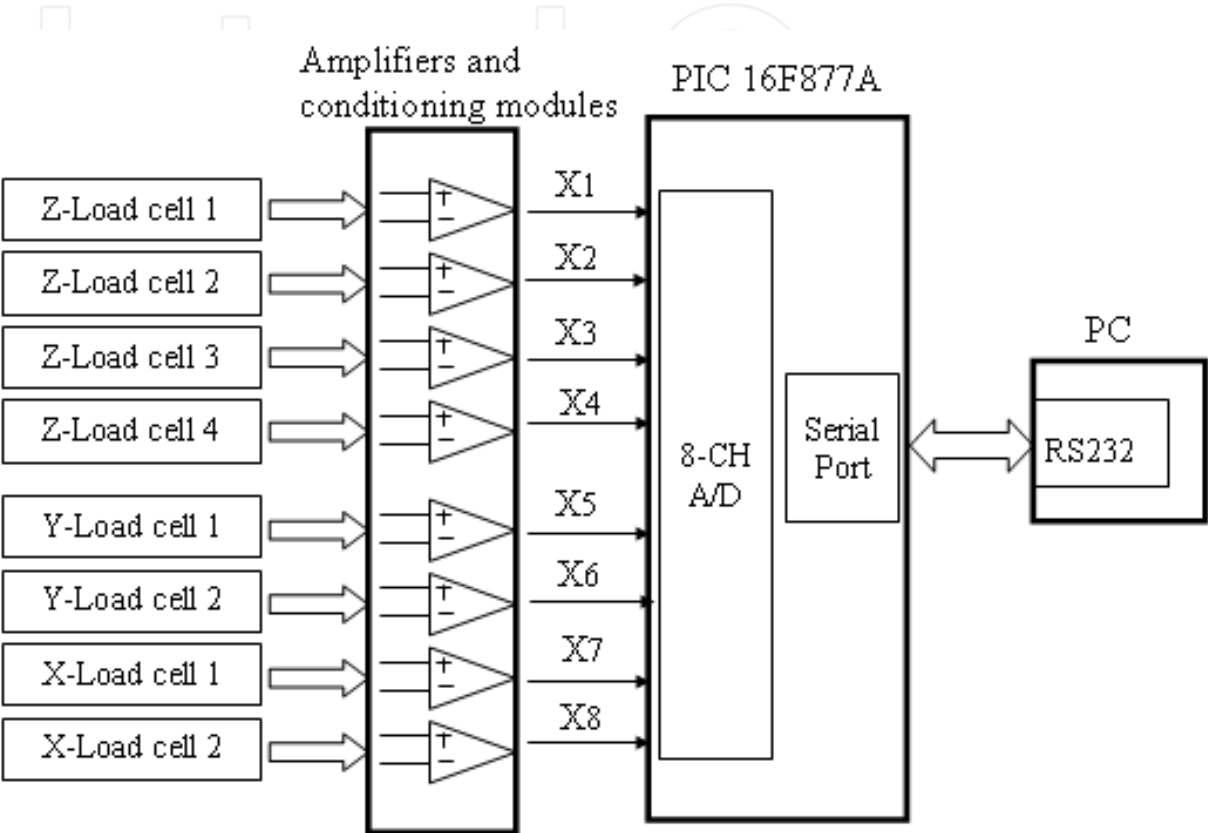

Fig. 6. Electrical hardware system of the sensor. The amplifier modules, conditioning circuits and microcomputer system were integrated on a based board, which was fixed in the mechanical structures of the sensor. The outputs of the amplifiers and conditioning modules (X_i) were used to calculate triaxial forces and moments applied on the sensor.

2.3 Prototype of Force Sensor

In order to achieve a high signal to noise ratio, amplifier modules, conditioning circuits and interface program were integrated into the force sensor. The large resistance strain gages (5000 ohm) of Vishay Micro-measurements were used, so the sensor system is low power consumed and can be powered using a small battery. Figure 7 shows the integrated sensor system and an interface software developed specially for monitoring the data obtained from the force sensor.

<div align="center">(a)   (b)</div>
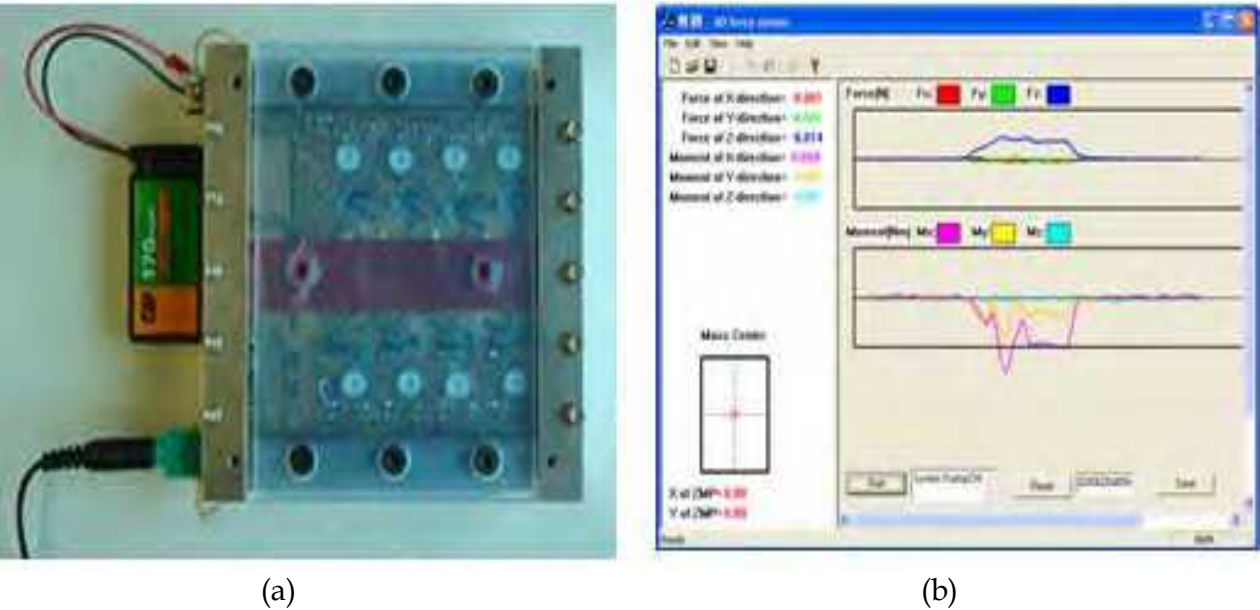
Fig. 7. Sensor system including a mechanical system, an electrical system and an interface software system. (a) The sensor hardware system can be power using a battery and communicate with a personal computer through a serial port of a micro-computer system; (b) An interface software for operation of the senor and sampling data from the sensor.

3. Wearable Motion Sensor

3.1 Motion Sensor System

As shown in Fig. 8, we developed a wearable motion sensor system which includes an eight-channel data recorder, a gyroscope and accelerometer combination unit, and two gyroscope units. The two gyroscope units are attached on the foot and thigh respectively, and the gyroscope and accelerometer combination unit is fixed on the shank, which is near to the ankle. The data-logger can be pocketed by subjects. The principle operation of the gyroscope is measurement of the Coriolis acceleration which is generated when a rotational angular velocity is applied to the oscillating piezoelectric bimorph. The inertial sensors can work under lower energy consumption (4.6 mA at 5V), so it is appropriate for ambulatory measurements. The signals from the gyroscopes and accelerometer are amplified and low-pass filtered (cutoff frequency: 25Hz) to remove the electronic noise. The frequencies outside the pass-band are filtered out because they are invalid for the study of human kinetics.

As shown in Fig. 9, three local coordinate systems were defined for the three sensor units, in which the sensing axis of the gyroscopes is along y-axis, and the z-axis is along the leg-bone. Three gyroscopes are used to measure angular velocities of leg segments of the foot, shank and thigh (ω_1, ω_2 and ω_3). The sensing axis (y-axis) of the gyroscopes is vertical to the medial-lateral plane so that the angular velocity in the sagittal plane can be detected. A bio-axial accelerometer is attached on the side of shank to measure two-directional accelerations along the tangent direction of x-axis (a_t) and the sagittal direction of z-axis (a_r). In this system the data obtained from accelerometer are fused with data collected from gyroscopes for a cycle re-calibration, through supplying initial angular displacements of the attached leg segment.
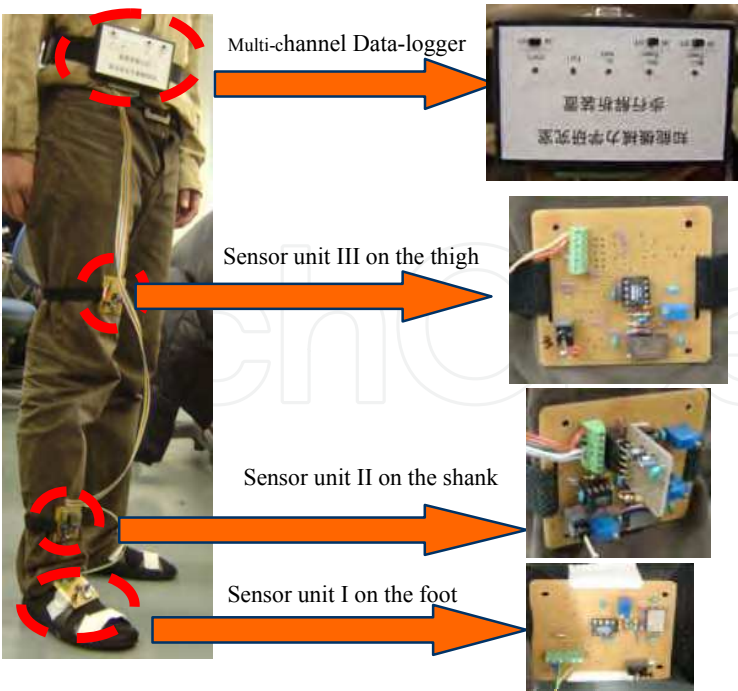
Fig. 8. Wearable motion sensor system. A strap system is designed for binding the sensor units to lower limb segments. Each sensor unit is attached to a strap. During walking, the strap is tied around the limb to secure the position of the sensor unit.
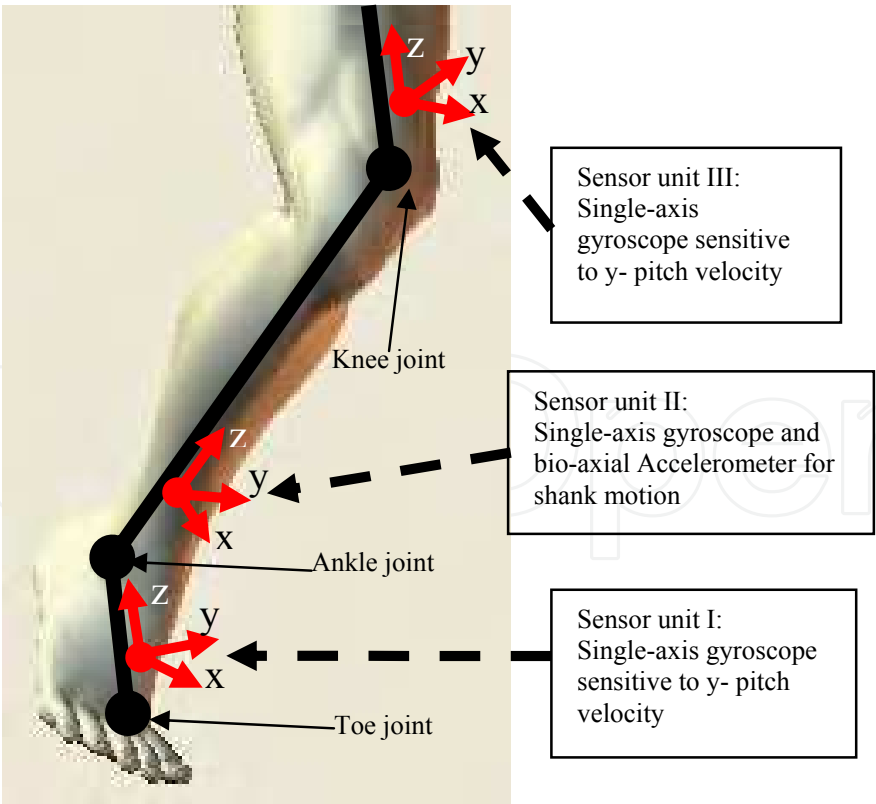

Fig. 9. Position and coordinates of the sensor units. In the local orientation coordinate of the sensor unit (x-, y- and z- axis), the y-axis denotes each joint's rocker axis, which is parallel to

the sensitive axis of the gyroscope, while x-axis and z-axis denote the unity vectors in the radial and tangential direction respectively.

A multi-channel data-logger was also specially designed for the wearable motion sensor system. A micro-computer (PIC 16F877A) was used to develop the pocketed data-logger, and the sampled data from the inertial sensors could be saved in a SRAM which can keep recording for five minutes. An off-line motion analysis can be performed by feeding data saved in the SRAM to a personal computer through a RS232 communication module. Since gyroscope (ENC-03J), accelerometer-chip (ADXL202) and the PIC system are all devices with a lower energy consumption, the wearable sensor system could be powered using a battery of 300mAh (NiMH 30R7H).

3.2 Calibration of Sensor Units

Complete architecture of a calibration system is showed in Fig. 10(a), and hardware devices of the system mainly include a data-logger (A/D card: Keyence NR-110), a potentiometer, a reference angle finder and a clamp (Fig. 10(b)).
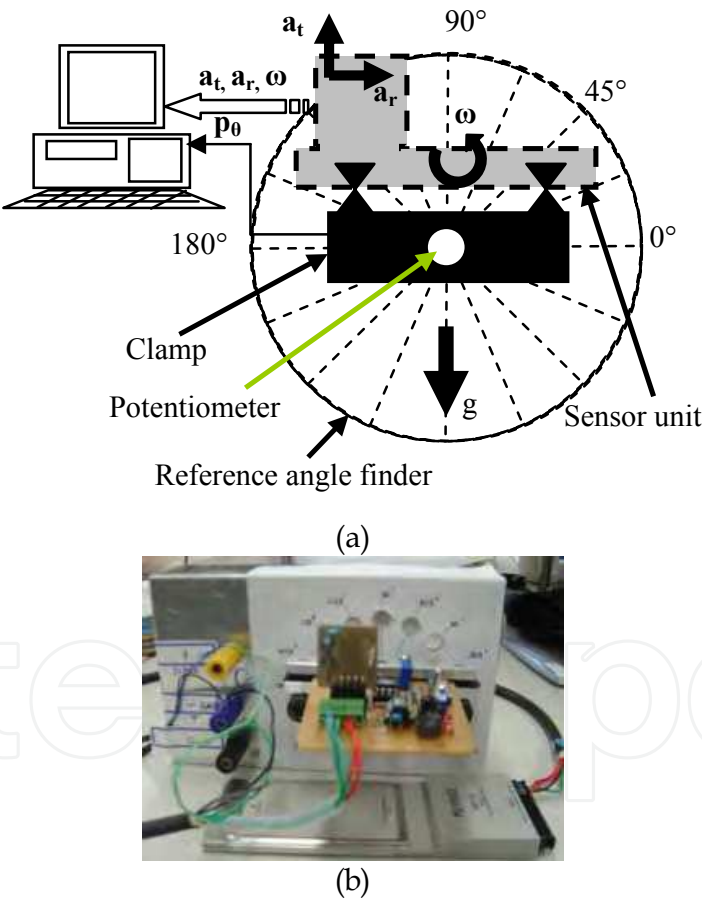

(a)

(b)

Fig. 10. (a) Architecture of the equipment for the calibration experiment of the sensor unit. A bio-axial accelerometer is used to measure two-directional accelerations of a_t and a_r, and p_θ is the output signal of the potentiometer which measures imposed rotational quantities and provides reference angular velocity quantities through a differential computing. Signal of the gyroscope in the sensor unit is defined as ω, and its positive direction is anticlockwise. The four signals of p_θ, ω, a_t and a_r are sampled into computer through the 12-bit A/D card. (b) Hardware devices with a mechanical case and an interface for the calibration of the sensor unit.

The sensor units are calibrated in static state and dynamic state respectively. First, the calibration of the accelerometer sensor is carried out during the static state. The accelerometer in sensor unit is subjected to different gravity vectors by rotating a based axis that is connected with a potentiometer. Second, the dynamic calibration is completed to calibrate the gyroscopes and test the accelerometer in a dynamic condition. In both cases the calibration matrixes are computed using the least squares method.

$[C_\theta]$ is calibration matrix for the angle position in (7). The matrix of the imposed quantities $[\theta]$ in a specific case can be recorded when the sensor unit is rotated to different positions on the angle finder plane; $[p_\theta]$ is the matrix of the quantities acquired from the potentiometer, in the specific positions of a sensor unit. Angular displacement $[\theta_r]$ can be calculated using (8), and angular velocity of the sensor unit is obtained through the differential computing of the angular positions in a serial time. Gravity acceleration g projected to the two sensitive axes (a_t and a_r) of the bio-axial accelerometer is estimated using (9) and (10).

$$[C_\theta] = [\theta][p_\theta]^T ([p_\theta][p_\theta]^T) - 1 \tag{7}$$

$$[\theta_r] = [C_\theta] \cdot [p_\theta] \tag{8}$$

$$A_t = -g \cdot \cos(\theta_r) \tag{9}$$

$$A_r = -g \cdot \sin(\theta_r) \tag{10}$$

$[C_{at}]$ and $[C_{ar}]$ are the calibration matrixes for the bio-axis accelerometer in (11) and (12), where $[A_t]$ and $[A_r]$ are the matrixes of the imposed quantities which were obtained when the sensor unit is subjected to different directional gravity vectors by rotating the sensor unit on the angle finder plane; $[a_t]$ and $[a_r]$ are the matrixes of the quantities assessed by the accelerometer in the sensor unit. (13) and (14) give summations of the subjected gravity g and the segment motion acceleration on the two sensitive axes using the output signals of the bio-axial accelerometer. Table 1 shows the data of a sensor unit from a representative calibration experiment.

$$[C_{at}] = [A_t][a_t]^T ([a_t][a_t]^T) - 1 \tag{11}$$

$$[C_{ar}] = [A_r][a_r]^T ([a_r][a_r]^T) - 1 \tag{12}$$

$$[A^{re}_r] = [C_{ar}] \cdot [a_r] \tag{13}$$

$$[A^{re}_t] = [C_{at}] \cdot [a_t] \tag{14}$$

$[C_g]$ in (15) is the calibration matrix for gyroscope sensor in the sensor units, where $[V_g]$ and $[p_\theta]$ are the matrixes of the quantities respectively acquired from the gyroscope and potentiometer in a serial time (t); $[C_\theta]$ is the calibration matrix for the angle position in (7). Angular position $[\theta_r]$ can be calculated using (8), and angular velocity of the sensor unit is obtained through difference computing of the angular positions in the serial time. Gravity acceleration g projected to the two sensitive axes (a_t and a_r) of the bio-axial accelerometer is estimated using (9) and (10).

$$[C_g] = [C_\theta][p_\theta]\left(\int V_g dt\left([\int V_g dt][\int V_g dt]^T\right)\right) - 1 \qquad (15)$$

Angle finder θ (Degrees)	Potentiometer p_θ (V)	Accelerometer	
		a_t (V)	a_r (V)
0	1.438	2.541	3.004
-22.5	1.355	2.798	2.943
-45	1.284	2.985	2.813
-67.5	1.209	3.108	2.602
-90	1.134	3.138	2.369
22.5	1.512	2.294	2.969
45	1.595	2.096	2.849
67.5	1.671	1.937	2.663
90	1.748	1.882	2.457

Table 1. Calibration results of a sensor unit.

3.3 Estimation of Segment Orientations

The loop frequency of the gait record is 100 Hz which is equal to the sensors sampling frequency, and the number of sampling time point is counted by an integer value i (i = 1, 2, 3….). The orientation of leg segment ($\theta(i)$) can be calculated by integral operator of the angular velocity ($\omega(i)$) of leg segment ((16) and (17)), which is directly measured using the wearable sensor units. The inclination of shank and thigh is set to zero in the initial period, while the inclination of foot is set to 90° at initial setting. Because the gyroscope in the sensor unit is a kind of inertial sensor that is affected by the drift errors when it is worn on the human body, the integral calculation in (16) must produce cumulated errors in the motion analysis of a multi-step walking trial.

$$\theta(i) = \theta(i-1) + (\omega(i-1) + \omega(i))\Delta t / 2 \qquad (16)$$

where

$$\theta(0) = \theta_0; \quad i = 1, 2, 3…. \qquad (17)$$

We define the gait cycle (walking gait cycle number k = 1, 2….) as the period from one stance phase of a foot to the next stance phase of the same foot. In every walking cycle, the time points of transition from loading response phase to mid stance phase, and transition from pre-swing to initial swing phase are defined (Parry, 1992). Based on the analysis of transition of the gait phases, the human motion analysis is implemented by calculating body segments' angular displacements using inertial sensors of gyroscopes and accelerometers. As shown in Fig. 11, we can primarily detect the mid stance phase just using gyroscope signals and raw integration results of gyroscope signals from the three sensor units ($\omega_t < 0$, $\omega_f = \varepsilon_\omega$, $\omega_s < 0$ and $\theta_s < 0$). Moreover, we find that the rotational angular velocities of

the shank and thigh are very small in the later interval of this phase, because the ankle is in a state of dorsiflexion, and the shank's rotational velocity is limited. Therefore, the accelerometer can be used for inclination measurement with respect to the gravity acceleration, when shank's sagittal direction A_r (18) and A_t (19) are mainly affected by the gravity acceleration's projection. Hence, we can make cycle calibration by measuring the initial angular orientation of the attached segment (the shank) using (20), and the foot orientation ($\theta_f^{\ m} = 0$) and the thigh orientation ($\theta_t^{\ m} = \theta_s^{\ m}$) are the initial calibration quantities for calculation of the foot and thigh orientations. Integral calculations are performed in every gait cycle, which can decrease the cumulated errors in longtime walking trials.
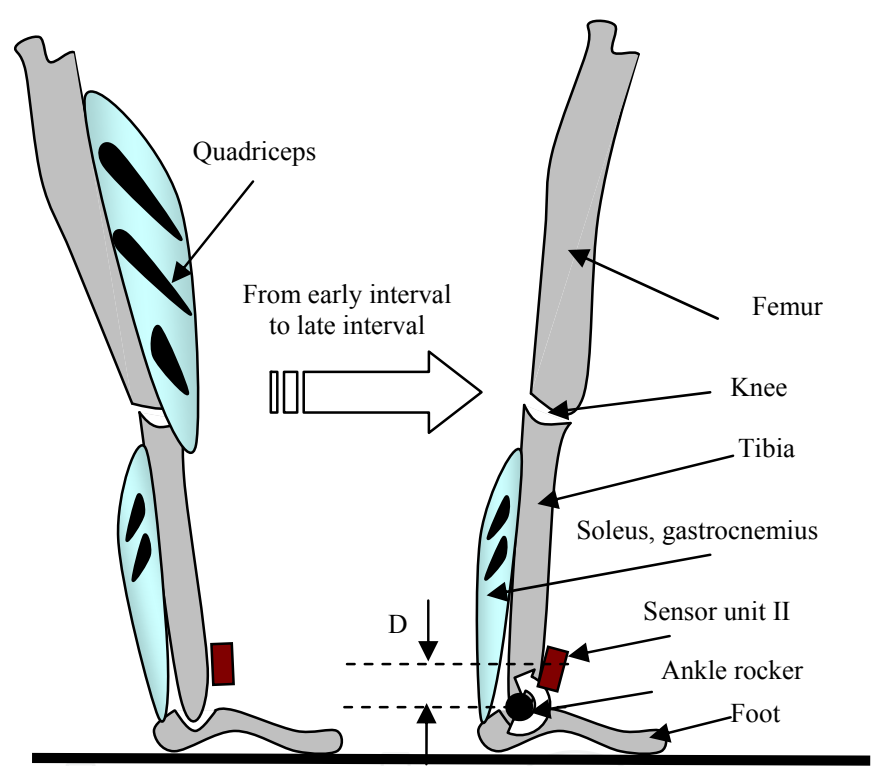

Fig. 11. Mid stance phase including the early and late intervals. The orientation calibration is implemented in the late interval of each mid stand. Early interval has body over mid foot with climb vertical, ankle neutral and foot flat, in which quadriceps and soleus muscles are in activity. Later interval has body over forefoot with continued heel contact, while ankle is in the state of dorsiflexion which limits the shank rotational velocity. A small distance between sensor unit II and ankle rocker is denoted using D (it is about 50mm). Moreover in the later interval, soleus and gastrocnemius are the only extensor muscles around tibia, which produces the least vibration effect on the accelerometer.

$$A_r = -g \cdot \sin(\theta_s^{\ m}) + D \cdot (\omega_s^{\ m})^2 \tag{18}$$

$$A_t = -g \cdot \cos(\theta_s^{\ m}) + D \cdot \dot{\omega}_s^{\ m} \tag{19}$$

$$\theta_s{}^m = \arctan(A_r / A_t) \tag{20}$$

However, the heel of some subjects (e.g. paralytic patient) may never contact the ground, and in this case the proposed direct inference algorithm can not be used for the cycle recalibration to decrease the integration errors. A linear regression method was developed to calculate drift errors coming from the digital integration, in which we supposed the error increase in a linear function. We let θ_i be the direct integration results by (16), and θ_m be reference static inclination angle measured using accelerometer by (20). The summary error ($\theta_e = \theta_i - \theta_m$) is obtained from a single walking trial during which subjects are required to walk along a straight leading line. Error estimation function ($\theta_e(i)$) is given as following equation based to a linear regression.

$$\theta_e(i) = \Delta t \cdot i \cdot (\theta_i - \theta_m) / t , \quad i = 1, 2, 3\ldots t \tag{21}$$

$$\theta_c(i) = \theta(i) - \theta_e(i) \tag{22}$$

where Δt is the sampling time and $\theta_c(i)$ was defined as the estimated angle after an error correction.

4. Calculation of Joint Moment

Based on the measurements of GRF and segment orientations using the two sensor systems, we can calculate lower limb's joint moments which are useful for evaluating in vivo forces of human body during gait. For calculation purposes, such as estimating joint moments of the ankle during loading response and terminal stance phases (Parry, 1992), all vectors including joint displacement vector, GRF vector and gravity vector have to be expressed in the same coordinate system, being the global coordinate system. The y-axis of the global coordinate system was chosen to represent the anterior-posterior direction of human movement, and the z-axis was made vertical, while the x-axis was chosen such that the resulting global coordinate system would be right-handed. The origin of the global coordinate system was fixed to a point around the anatomical center of the ankle when the wearable force sensor was worn under the foot. The GRF and the moments measured using the wearable force sensor are expressed by the vectors in (23), and the coordinates of center of pressure (CoP) ${}^g x_{CoP}$ in the global frame is calculated using the following equation:

$$
{}^g F_{GRF} = \begin{pmatrix} {}^g F_x \\ {}^g F_y \\ {}^g F_z \end{pmatrix} \quad {}^g M_{GRF} = \begin{pmatrix} {}^g M_x \\ {}^g M_y \\ {}^g M_z \end{pmatrix} \quad {}^g x_{CoP} = \begin{pmatrix} \dfrac{{}^g M_y}{{}^g F_z} \\ \dfrac{{}^g M_y}{{}^g F_z} \\ 0 \end{pmatrix} \tag{23}
$$

The ankle, knee and hip joint moments in the global coordinates system can be calculated using the inverse dynamic method (Hof, 1992; Zheng et al., 2008)

$$
{}^{g}M_{k,k+1} = -({}^{g}r_{CoP} - {}^{g}r_{k,k+1}) \times F_{GRF} - \sum_{i=1}^{k} \left[({}^{g}r_i - {}^{g}r_{k,k+1}) \times m_i \cdot g \right]
$$

$$
+ \sum_{i=1}^{k} \left[({}^{g}r_i - {}^{g}r_{k,k+1}) \times m_i \cdot a_i \right] + \sum_{i=1}^{k} \frac{d}{dt}\left(I_i \cdot \dot{\theta}_i \right) \quad , k=1, 2, 3, \quad (24)
$$

where ${}^{g}M_{1,2}$, ${}^{g}M_{2,3}$ and ${}^{g}M_{3,4}$ represent the ankle, knee and hip joint moments respectively. ${}^{g}r_{CoP}$ is referred as the position vector pointing from the origin of the global coordinate system to the CoP. ${}^{g}r_1$, ${}^{g}r_2$ and ${}^{g}r_3$ are the position vectors from the origin of the global coordinates system to the centers of the ankle, knee and hip joints. ${}^{g}r_{1,2}$, ${}^{g}r_{2,3}$ and ${}^{g}r_{3,4}$ are the position vectors from the origin of the global coordinates system to the center of mass (CoM) of the foot, shank and thigh respectively. The mass of the foot, shank and thigh was defined as m_1, m_2 and m_3 respectively. a_1, a_2 and a_3 are the accelerations of the CoM of the foot, shank and thigh respectively. I_1, I_2 and I_3 are the inertia moments of the foot, shank and thigh respectively. The angular velocities of the foot, shank and thigh were obtained by the differential operators ($\dot{\theta}_1$, $\dot{\theta}_2$ and $\dot{\theta}_3$).

5. Experiment Study

5.1 Experiment Method
To validate the sensor system performance we have compared the quantitative results of the sensor system with the measurements obtained with a commercial optical motion analysis system Hi-DCam (NAC image technology. Japan). The commercial motion analysis system can track and measure three-dimensional (3-D) trajectories of retro-reflective markers placed on the subject's body, as shown in Fig. 12. The cameras with a sampling frequency of 100 Hz were used to track the marker positions with an accuracy of about 1 mm. A stationary force plate of EFP-S-2KNSA12 (Kyowa co. Japan) was also used as a reference sensor to validate the measurement of the developed force sensor. In our experiment, these sensor systems simultaneously worked in the measurements of human force and motion. The data from the reference sensor systems and our developed sensor systems were sampled at the same time, and were compared.
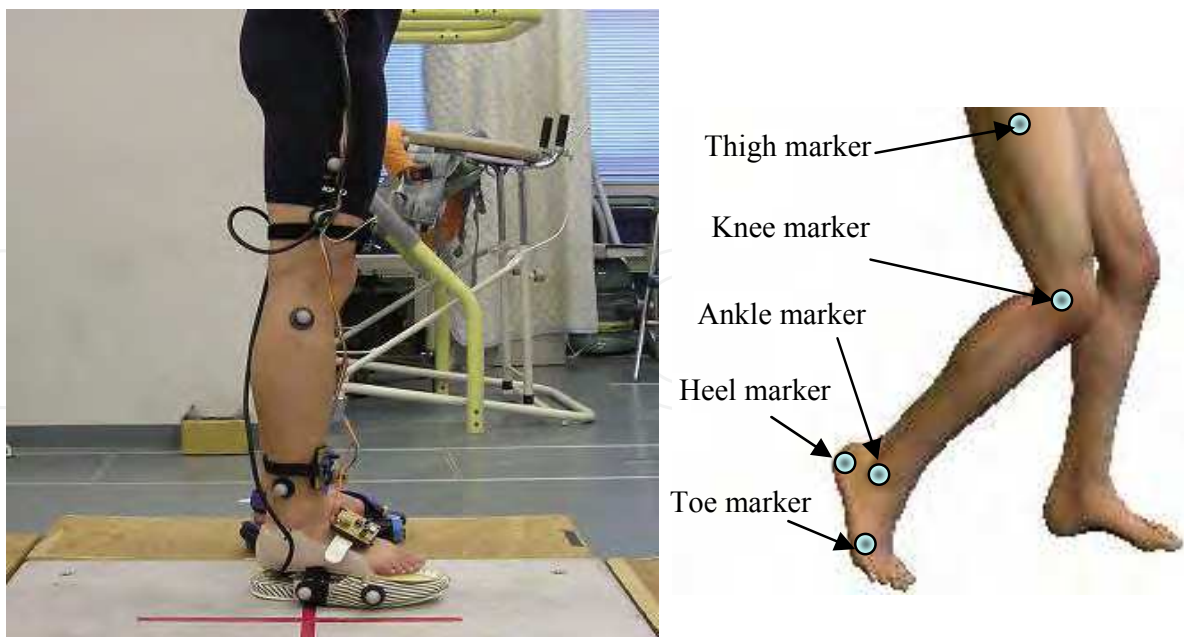
Fig. 12. Verification experiment system and positions of the retro-reflective markers

The root of the mean of the square differences (RMS) was used to compare the closeness in amplitude of the two sensor measurement results. The percent error (PE) was calculated as the ratio between the RMS errors to the average peak-to-peak amplitude of the reference measurements.

$$RMS = \sqrt{\left(\frac{1}{n}\sum(F-F_r)^2\right)} \qquad (25)$$

Ten healthy subjects (eight men and two women: age=28.1±2.0years, height=169.2±4.2cm, weight=66.3±9.2kg) were required to wear the developed sensor system in experiment tests. Segmental mass and inertial moment parameters of the lower extremities of the subjects could be estimated using the empirical regression method (Zatsiorsky and Seluyanov, 1983). The length of the thigh, shank and foot of the subjects is 0.4165±0.0224m, 0.3715±0.03m, and 0.2453±0.008m respectively. The mass of the foot, shank and thigh is 0.7355±0.0635kg, 3.1043±0.3902kg and 7.6924±0.8436kg respectively. The ratio of the center of gravity was calculated as the mean value of the percentage of the segment length measured from the proximal end. The mean of the ratio of the foot, shank and thigh is 59.5%, 40.6% and 0.475% respectively for the male subjects, while 59.4%, 41% and 45.8% respectively for the female subjects. The inertial moment of the foot, shank and thigh is 0.00037732±0.00000365kgm², 0.0302±0.0101kgm² and 0.0973±0.0139kgm² respectively.

5.2 Experiment Results: GRF and Segmental Orientations
As shown in Fig. 13 (a)-(c), the comparisons of the three components of GRF measured using the wearable sensor systems and the stationary force plate system were demonstrated in a representative trial. The results of GRF were normalized with respect to the body weight.

The results show a good correspondence between two methods, which is confirmed by comparison analysis of the GRF (see Fig. 13(d)) and errors analysis of the GRF (see Fig. 13 (e)), and RMS differences by the ten subjects' trials of 0.045±0.003 N/N (mean ± standard deviation), which corresponds to 4.26±0.34% of the maximal GRF magnitude. A separate analysis of each component of the GRF results for the vertical component in an RMS difference of 0.046±0.002N/N, being 4.8±0.2% of the maximal GRF magnitude, or 4.2±0.2% of the maximal vertical components. For the x-directional component of the horizontal GRF, RMS difference is 0.011±0.008N/N, being 1.07±0.91% to the maximal GRF magnitude, or 10.3±2.2% to the maximal x-directional component. For the y-directional component of the horizontal GRF, RMS difference is 0.014±0.002N/N, being 1.17±0.12% to the maximal GRF magnitude, or 10.1±3.6% to the maximal y-directional component of GRF.
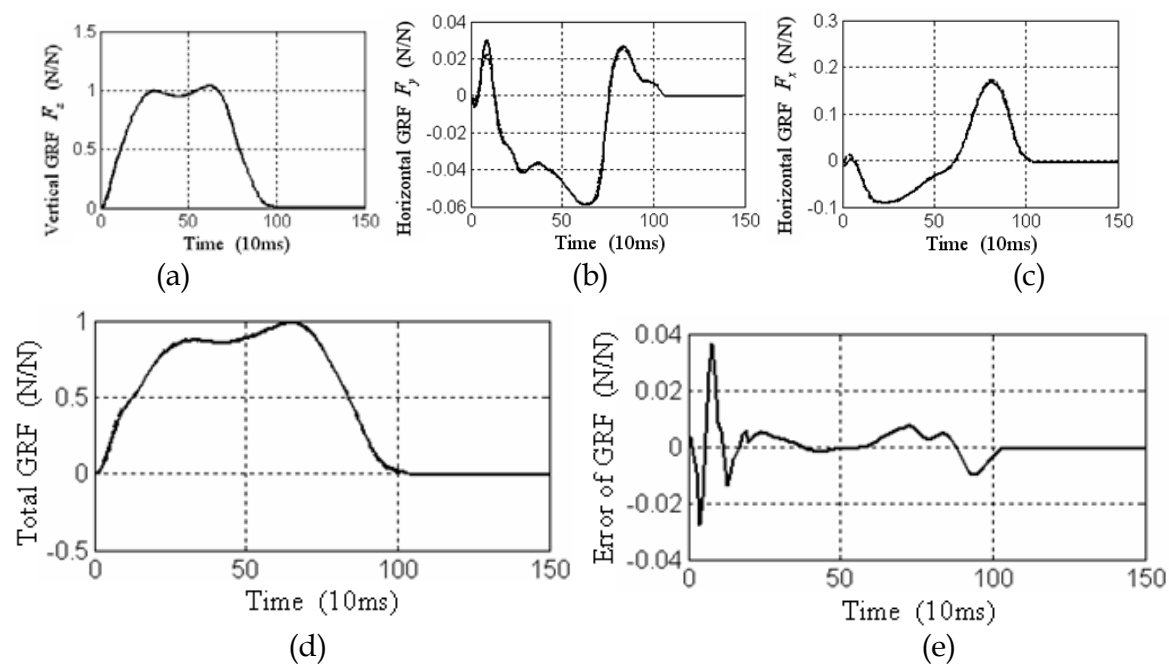
Fig. 13. Triaxial GRF measured by the wearable sensor systems (solid line) and the force plate (dashed line). (a) The vertical components: F_z. (b) The horizontal component: F_y. (c) Horizontal component: F_x. (d) The total GRF. (e) Error of GRF between the two measurement systems.

The estimation of the position of the CoP is shown in Fig. 14. The trajectories agree well, and RMS difference between the two methods was 10.4±1.2mm, corresponding to 3.7±0.5% of the length of the instrumented shoe.
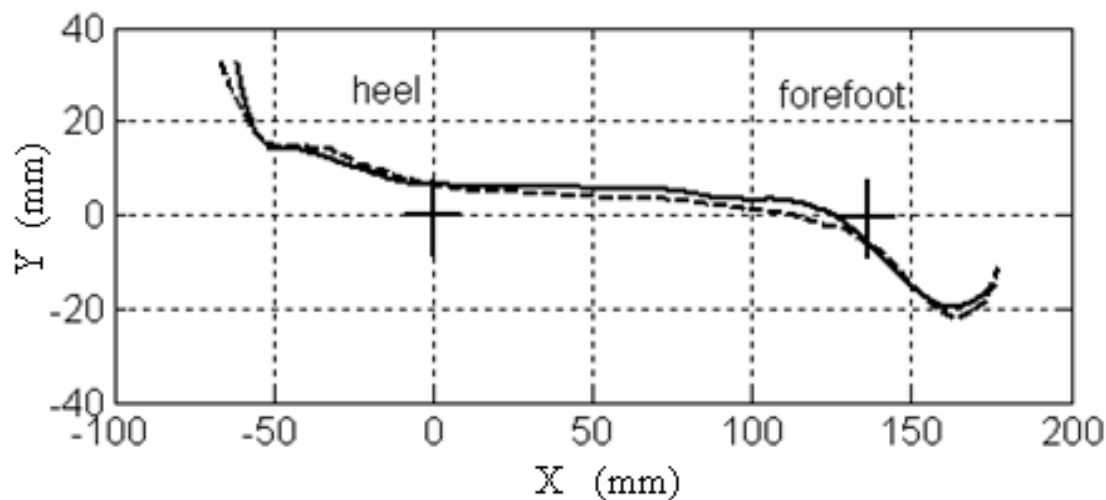
Fig. 14. Center of pressure (CoP) measured by the wearable sensor system (solid line) and the stationary force plate (dashed line) in the global coordinate system.

(a)   (b)   (c)
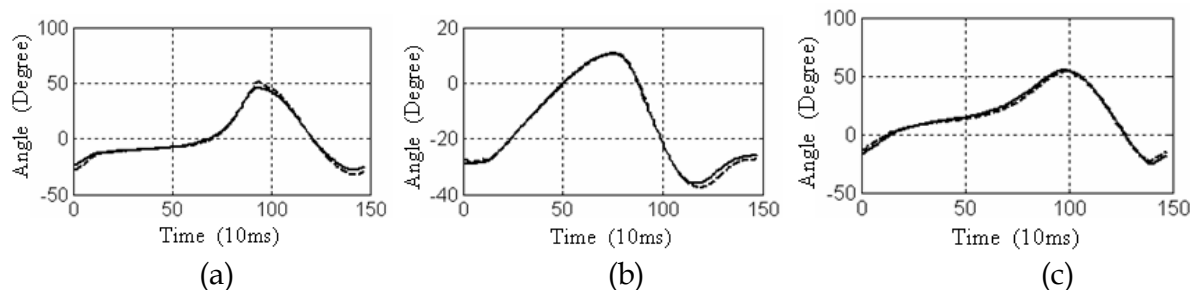
Fig. 15. Segmental angular displacements measured by the wearable motion sensor system (solid line) and the Hi-DCam camera system (dashed line). (a) Foot angular displacements. (b) Shank angular displacements. (c) Thigh angular displacements.

As shown in Fig. 15, the segmental angular displacements estimated using the wearable sensor system and Hi-DCam camera system were also compared. For the foot angular displacement, the RMS difference between the results estimated using the two systems was calculated as 2.91±0.12degrees, being 5.6±0.35% of the maximal magnitude of the foot angular displacements. For the shank angular displacement, the RMS difference between the two methods is 2.61±0.93degrees, being 4.71±1.4% of the maximal magnitude of the shank angular displacement. For the thigh angular displacement, the RMS difference between the two methods is 1.3±0.39degrees, being 4.71±2.05% of the maximal magnitude of the thigh angular displacement.

5.3 Experiment Results: Joint Moments

The comparison results of the joint moments of the ankle, knee and hip in the sagittal plane between the two measurement systems are shown in Fig. 16. The RMS difference of the ankle joint moments calculated using the two systems is 2±0.34Nm, being 5.4±0.7% of the maximal magnitude of the ankle joint moments during a whole gait cycle. The RMS difference of the knee joint moments calculated using the two systems is 7.2±1.34Nm, being 6±0.32% of the maximal magnitude of the knee joint moments. The RMS difference of the

hip joint moments calculated by using the two systems is 11.2±1.3Nm, being 6.1±0.25% of the maximal magnitude of the hip joint moments.

(a)   (b)   (c)
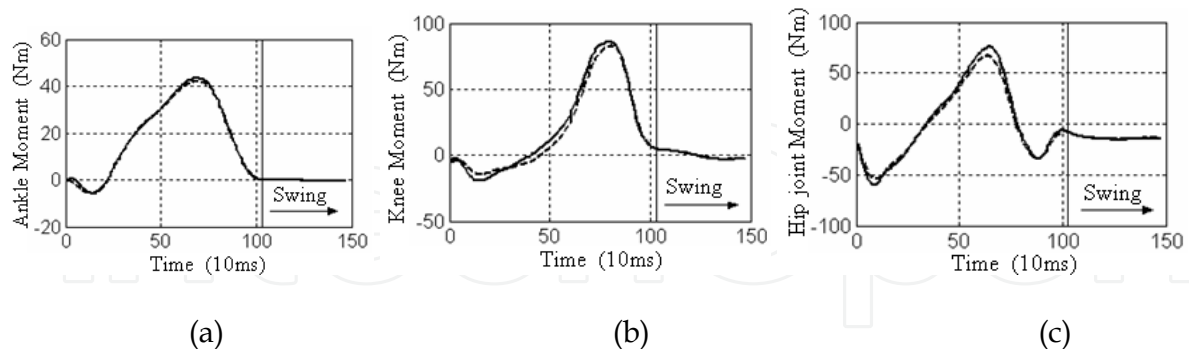
Fig. 16. Joint moments estimated by the wearable sensor systems (solid line), and the force plate & Hi-DCam camera systems (dashed line). Ankle plantarflexor, knee extensor, and hip flexor are positive, and ankle dorsiflexion, knee flexor, and hip extensor are negative. (a) Ankle joint moments. (b) Knee joint moments. (c) Hip joint moments.

6. Conclusion

A new wearable sensor system was developed for measuring tri-directional ground reaction force (GRF) and segment orientations. A stationary force plate can not measure more than one stride; moreover, in studies of stair ascent and descent measurements, a complex system consisting of many stationary force plates and a data fusion method must be constructed (Stacoff et al., 2005; Della and Bonato, 2007). The wearable sensor system proposed in this chapter can be applied to successive walking trials in a number of non-laboratory environments, because of its lower-cost, small size and lower effects on human movements. The joint moment estimations of the ankle, knee and hip joints using the measurements of the wearable sensor system is an application study. The joint moment data should be helpful for understanding the cause of certain gait abnormalities and the motion mechanism of human walking, when we combine it with the other measurements, such as 3D joint angles and electromyography. In the verification experiments, we measured the triaxial GRF, coordinates of CoP, and lower limbs' angular displacements, and caluculated joint moments using the measurments of the wearable sensor system and the force plate & optical camera system. The analysis of the RMS differences between the two systems was implemented, and the results of the RMS differences demonstrated that the force and motion measurement results and the joint moment estimation results have high consistence between the two systems. In the next step, based on the estimated joint moments, we will use the wearable sensor systems to estimate muscle tension forces by a static optimization method and a musculoskeletal model of the lower limb, because muscle tension forces provide further details about human physiological data during gait.

7. References

Aminian, K.; Najafi, B.; Bula, C.; Leyvraz, P.F. & Robert, P. (2002). Spatio-temporal parameters of gait measured by an ambulatory system using miniature gyroscopes. *Journal of Biomechanics,* vol. 35, pp. 689-699, ISSN: 0021-9290.

Coley, B.; Najafi, B.; Paraschiv-Ionescu, A. & Aminian, K. (2005). Stair climbing detection during daily physical activity using a miniature gyroscope. *Gait and Posture,* vol. 22 (4), pp. 287-294, ISSN: 0966-6362.

Della, U. & Bonato, P. (2007). A novel design for an instrumented stairway. *Journal of Biomechanics*, vol. 40, pp. 702-704, ISSN: 0021-9290.

Faivre, A.; Dahan, M.; Parratte, B. & Monnier, G. (2004). Instrumented shoes for pathological gait assessment. *Mechanics Research Communications*, vol. 31, pp. 627-632, ISSN: 0093-6413.

Hof, A. L. (1992). An explicit expression for the moment in multibody systems, *Journal of Biomechanics*, Vol. 25, No. 10, pp. 1209-1211, ISSN: 0021-9290.

Hwang, E.S.; Yoon, Y.R.; Yoon, H.R.; Shin, T.M. & Kim, Y.J. (2008). Flexible contact force sensing device using metal/polymer multilayer structure for robotic applications. *Sensors and Materials,* vol. 20, pp. 55-69, ISSN: 0914-4935.

Jasiewicz, J.M.; Allum, J.H.J.; Middleton, J.W.; Barriskill, A.; Condie, P.; Purcell, B. & Li, R.C.T. (2006). Gait event detection using linear accelerometers or angular velocity transducers in able-bodied and spinal-cord injured individuals. *Gait and Posture,* vol. 24, pp. 502-509, ISSN: 0966-6362.

Lau, H. & Tong, K. (2008). The reliability of using accelerometer and gyroscope for gait event identification on persons with dropped foot. *Gait and Posture,* vol. 27, pp. 248-257, ISSN: 0966-6362.

Liedtke, C.; Fokkenrood, S.A.W.; Menger, J.T.; Kooij, H. & Veltink, P.H. (2007). Evaluation of instrumented shoes for ambulatory assessment of ground reaction forces. *Gait and Posture*, vol. 26, pp. 39-47, ISSN: 0966-6362.

Najafi, B.; Aminian, K.; Loew, F.; Blanc, Y. & Robert, P.A. (2002). Measurement of stand-sit and sit-stand transitions using a miniature gyroscope and its application in fall risk evaluation in the elderly. *IEEE Transactions on Biomed. Eng.,* vol. 49, pp. 843-851, ISSN: 0018-9294.

Parry, J. (1992). *Gait analysis normal and pathological function*, Slack Incorporated, pp. 149-158, ISBN: 9781556421921.

Sabatini, A.M.; Martelloni, C.; Scapellato, S. & Cavallo, F. (2005). Assessment of walking features from foot inertial sensing. *IEEE Transactions on Biomed. Eng.,* vol. 52 (3), pp. 486-494, ISSN: 0018-9294.

Schepers, H.M.; Koopman, H. F. J. M. & Veltink, P.H. (2007). Ambulatory assessment of ankle and foot dynamics. *IEEE Trans. Biomed. Eng.*, vol. 54, pp. 895-900, ISSN: 0018-9294.

Stacoff, A.; Diezi, C.; Luder, G.; Stussi, E. & Quervain, I.A. (2005). Ground reaction forces on stairs: Effects of stair inclination and age. *Gait and Posture*, vol. 21, pp. 24-38, ISSN: 0966-6362.

Stacoff, A.; Quervain, I.A.K.d.; Luder, G.; List, R. & Stussi, E. (2007). Ground reaction forces on stairs. Part II: Knee implant patients versus normal. *Gait and Posture*, vol. 26, pp. 48-58, ISSN: 0966-6362.

Valdastri, P.; Roccella, S.; Beccai, L.; Cattin, E.; Menciassi, A.; Carrozza, M.C. & Dario, P. (2005). Characterization of a novel hybrid silicon three-axial force sensor. *Sensors & Actuators: A. Physical*, vol. 123-124, pp.249-257, ISSN: 0924-4247.

Veltink, P.H.; Liedtke, C.; Droog, E. & Kooij, H. (2005). Ambulatory measurement of ground reaction forces. *IEEE Trans Neural Syst Rehabil Eng.*, vol. 13, pp. 423–527, ISSN: 1534-4320.

Yavuzer, G., Oken, O., Elhan, A., Stam, H.J., 2008, "Repeatability of lower limb three-dimensional kinematics in patients with stroke," *Gait and Posture*, 27(1), pp. 31-35, ISSN: 0966-6362.

Zatsiorsky, V. M. & Seluyanov, V. N. (1983). The mass and inertia characteristics of the main segments of the human body, In: *Biomechanics VIII-B,* Edited by Matsui, H. & Kobayashi, K., pp. 1152-1159. Human Kinetics Publishers, Chamapaign, IL.

Zhang, K.; Sun, M.; Lester, D.K.; Pi-Sunyer, F.X.; Boozer, C.N. & Longman, R.W. (2005). Assessment of human locomotion by using an insole measurement system and artificial neural networks. *Journal of Biomechanics*, vol. 38, pp. 2276-2287, ISSN: 0021-9290.

Zheng, R.; Liu, T.; Inoue, Y.; Shibata, K.; Liu, K.; (2008). Kinetics analysis of ankle, knee and hip joints using a wearable sensor system, *Journal of Biomechanical Science and Engineering*. Vol. 3(3), pp.343-355, ISSN: 1880-9863.

Mechatronic Systems Applications

Edited by Annalisa Milella Donato Di Paola and Grazia Cicirelli

Mechatronics, the synergistic blend of mechanics, electronics, and computer science, has evolved over the past twenty five years, leading to a novel stage of engineering design. By integrating the best design practices with the most advanced technologies, mechatronics aims at realizing high-quality products, guaranteeing at the same time a substantial reduction of time and costs of manufacturing. Mechatronic systems are manifold and range from machine components, motion generators, and power producing machines to more complex devices, such as robotic systems and transportation vehicles. With its twenty chapters, which collect contributions from many researchers worldwide, this book provides an excellent survey of recent work in the field of mechatronics with applications in various fields, like robotics, medical and assistive technology, human-machine interaction, unmanned vehicles, manufacturing, and education. We would like to thank all the authors who have invested a great deal of time to write such interesting chapters, which we are sure will be valuable to the readers. Chapters 1 to 6 deal with applications of mechatronics for the development of robotic systems. Medical and assistive technologies and human-machine interaction systems are the topic of chapters 7 to 13.Chapters 14 and 15 concern mechatronic systems for autonomous vehicles. Chapters 16-19 deal with mechatronics in manufacturing contexts. Chapter 20 concludes the book, describing a method for the installation of mechatronics education in schools.

INTECH
open science | open minds